

Quasi-Periodic Bifurcations and Chaos

Taoufik Bakri ¹ and Ferdinand Verhulst ^{2,*}

¹ TNO Sustainable Urban Mobility & safety, PO Box 96800, 2509 JE The Hague, The Netherlands; taoufik.bakri@tno.nl

² Mathematisch Instituut, PO Box 80.010, 508TA Utrecht, Netherlands; f.verhulst@uu.nl

* Correspondence: e-mail@e-mail.com; Tel.: (optional; include country code; if there are multiple corresponding authors, add author initials) +xx-xxxx-xxx-xxxx (F.L.)

† Current address: Affiliation.

‡ These authors contributed equally to this work.

Abstract: A natural phenomenon in applications is the interaction of quasi-periodic solutions of dynamical systems in a dissipative setting. We study the interactions of two of such systems based on construction of a nonlinear oscillator with thermostatic (energy) control. This leads to the emergence of complexity, torus-doubling and chaos. We find canards, single 2- and 3-tori, chaos and hyperchaos. Detailed analysis is possible in the case of small oscillations and small interactions. Large-scale phenomena are studied by the construction of charts of parameter space using Lyapunov-exponents.

Keywords: quasi-periodicity; bifurcation; tori; chaos; Lyapunov-exponent

1. Introduction

Interactions of 2 or more nonlinear oscillators produce in general complex dynamics with periodic solutions, tori, tori-doubling and chaos. A natural feature in real-life models is that the interactions are quasi-periodic which means that the individual components have frequencies that are incommensurable. See for a discussion of diophantine frequency vectors and the measure of Cantor sets in 2-frequency systems [8] with also many references inspired on the conservative setting leading to families of invariant tori; we mention in this setting the basic paper [7].

Our focus is different from KAM-theory and with some exceptions also from dissipative KAM-theory as we are especially interested in the practical context where we start with dissipative systems that are subsequently perturbed and lead to complex behaviour. This can produce bifurcations of isolated tori and their qualitative changes. As we shall see we will consider for our analysis a system with damping and thermostatic control, combination of 2 of such systems adds forcing and bifurcation phenomena.

Multifrequency oscillations arise in many applications of various disciplines as mechanical engineering, laser systems, electronic circuits; for a useful list of such applications in many fields see [14] (in particular references [1-23]), and [27]. In [14] and [27] the emphasis is on the construction of charts of Lyapunov-exponents for interacting self-excited systems. Such numerically obtained charts yield enormous inspiration for further analysis. Important analytic tools are mathematically sound approximation techniques, see for instance [34] (ch. 9), and bifurcation theory, see for instance [15]. It is generally known that an equilibrium of a system of differential equations that for a certain parameter value has 2 imaginary eigenvalues can generate a periodic solution by Poincaré-Andronov-Hopf bifurcation. The generating periodic solution is a guiding center of the torus. In a similar way a periodic solution that is characterised by 2 imaginary eigenvalues or



Received:

Revised:

Accepted:

Published:

Citation: Lastname, F.; Lastname, F.; Lastname, F. Title. *Mathematics* **2025**, *1*, 0. <https://doi.org/>

Copyright: © 2025 by the authors. Licensee MDPI, Basel, Switzerland. This article is an open access article distributed under the terms and conditions of the Creative Commons Attribution (CC BY) license (<https://creativecommons.org/licenses/by/4.0/>).

corresponding Lyapunov exponents may generate a torus by Neimark-Sacker bifurcation. In the case of quasi-periodic interactions it is natural to discover and identify tori. Usually they branch off equilibria and periodic solutions. The first question is then whether they are normally hyperbolic or not. Starting with an autonomous system of ODEs there will be at least 1 Lyapunov exponent zero. Are there more zeros and, when varying parameters, do we find Hopf and other bifurcations, tori-doubling and cascades of such phenomena leading to chaos?

Apart from normal form theory and averaging, we used numerical methods as implemented in MATHEMATICA, MATLAB, MATCONT. The last one uses continuation methods to follow parameter changes that cause bifurcations. It turns out that the hybrid combination of analytic and numerical tools can be very inspiring.

What is New?

To obtain insight in dissipative quasi-periodic bifurcations we modify in section 2 an important thermostatic control problem (Sprott A), a chaotic system formulated in [26] and [13]. Earlier studies of Sprott A giving more insight are [19]-[20], in [3]-[4] the thermostatic control problem of [26] is linked to tori families as is well-known for conservative systems. The context of conservative systems is classical and interesting but in general less suitable for applications in engineering and other science fields that involve dissipation.

A new step in section 2 is to introduce a 2-dimensional basic oscillator with periodic solutions that are asynchronous; when adding a 1-dimensional thermostatic control and assuming small oscillations we find canard behaviour. Admitting larger amplitudes we can identify periodic solutions in a resonance manifold by slow-fast dynamics.

In section 3 we consider the 6-dimensional interaction of 2 such components. If dissipation and thermostatic control are excluded we have a system with 2 interacting quasi-periodic oscillators. To study the bifurcations of this system with dissipation, interaction and control is the central part of this paper. When considering small oscillations and small interactions one can use averaging to find single tori with 1 or 2 zero Lyapunov-exponents. Combining canard initial values the solutions converge to a flattened torus. Torus doubling arises leading to a cascade of torus doublings. To obtain an overview of phenomena we constructed charts for larger values of dissipation and interactions. For each value of 2 parameters one obtains either a 2-torus, a 3-torus, chaos or hyperchaos.

Conclusions and a discussion finish the main part of the paper.

Appendix A lists the results that carry directly over from the 2-components case to systems with n components.

2. One Component Oscillations with Energy Control

An autonomous one degree-of-freedom nonlinear oscillator with damping can be described by:

$$\ddot{q} + b\dot{q} + q + f(q) = 0, \quad (1)$$

with dissipation parameter $b \geq 0$. A dot above a variable is short for differentiation with respect to time. We assume that the function $f(q)$ is analytic, near $q = 0$ it has a power series expansion starting with quadratic terms. If $b = 0$ we have no energy loss, in this case the oscillator has the energy integral

$$E = \frac{1}{2}(q^2 + \dot{q}^2) + \int_0^q f(s)ds, \quad (2)$$

with E a constant parameter depending on the initial conditions. In the conservative case ($b = 0$) eq. (1) has an infinite number of periodic solutions with period depending on $E = E_0$. If $f(q)$ is deleted in the equation we have the synchronised case of the harmonic

equation with all periods equal (2π).

In chemical physics, see [31], one introduces a thermostatic control by adding an equation controlling the dissipative term $b\dot{q}$ by a new variable z , replacing $b\dot{q}$ by $bz\dot{q}$. The control $z(t)$ can become negative producing excitation if the energy (or another suitable quantity) characterising the oscillator is smaller than a chosen threshold, $z(t)$ can become positive causing increased damping if the energy is larger than the threshold. Apart from using the energy of a nonlinear equation we have with eq. (1) the natural case of periodic solutions with period dependent on the energy. To fix ideas we will choose

$$f(q) = cq^3.$$

The thermostatic control z for the energy leads to the system:

$$\begin{cases} \ddot{q} + bz\dot{q} + q + cq^3 = 0, \\ \dot{z} = q^2 + \dot{q}^2 + \frac{c}{4}q^4 - a, \end{cases} \quad (3)$$

with parameters $a, c > 0$. The expression $q^2 + \dot{q}^2 + \frac{c}{4}q^4$ is not exactly representing the energy but measures the energy.

In [4] system (3) was studied in the case $c = 0$, this system is called Sprott B. We note that for small oscillations (q, \dot{q} small) the solutions of the Sprott B system will to first approximation describe the solutions of system (3) correctly; this will be made more precise later on. Replacing the equation for z by

$$\dot{z} = \dot{q}^2 - a,$$

with $c = 0$ the system is called Sprott A, see [26], [13], [3] and many references there. Choosing $c > 0$ implies that we have no saddle equilibrium in the conservative oscillator ($b = 0$). Choosing c negative would change the dynamics for larger values of the initial energy; in fig. 1 we illustrate this for $c = 1$ where all solutions are periodic and $c = -1$ producing saddles in the phase-plane.

Stability and Lyapunov-exponents

In the sequel we will look for periodic solutions and their stability. In section 5.4 of [32] it is shown that if we have located a periodic solution $\phi(t)$ of an autonomous system (as (3)), linearisation near $\phi(t)$ produces as one solution of the linearised system $\dot{\phi}(t)$. In the case of system (3) this means that one of the three Lyapunov-exponents will be zero.

Exact analytical solutions

We note that system (3) has no equilibria (critical points of the vector field). We find an unbounded invariant manifold if $x(0) = \dot{x}(0) = 0$ with dynamics given by

$$z(t) = z(0) - at.$$

The following result is well known.

Lemma 1. Consider system (3) with $b = 0$; as $c > 0$ all solutions $q(t)$ are periodic but not synchronous.

A few examples of energy E_0 with $b = 0, c = 1$ and corresponding period P are: $(E_0, P) = (0.01, 6.4), (0.125, 5.8), (0.5, 5.1), (1.125, 4.4), (2, 4), (4.5, 3.3), (8, 3), (12.5, 2.7)$. The cycles in the phase-plane are shown in fig. 1 (left); increasing E_0 shortens P .

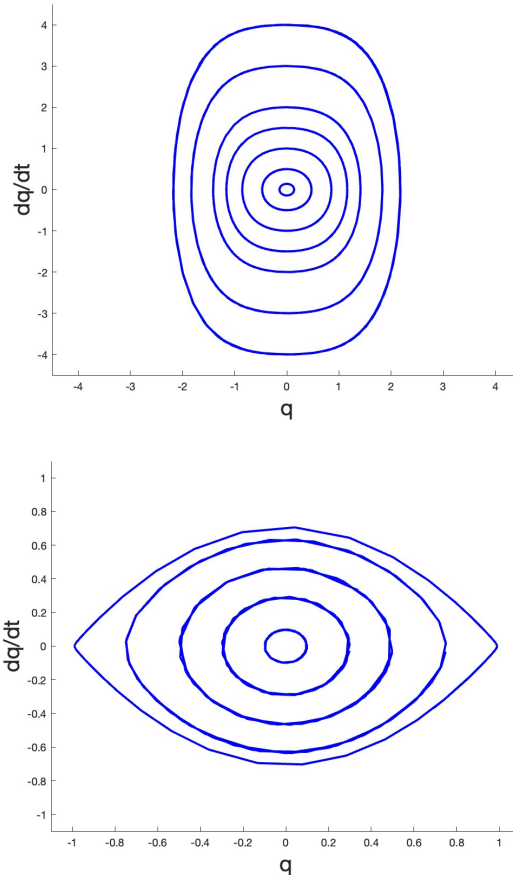


Figure 1. Phase-plane with periodic solutions of eq. $\ddot{q} + q + cq^3 = 0$. Left the case $c = 1$. Right the case $c = -1$ producing 2 saddle equilibria at $q = \pm 1, \dot{q} = 0$ with inside the 2 heteroclinic connections periodic solutions.

Time-reversal

We will use the concept of time-reversibility of system (3). Put $\dot{q} = v$. The system is characterised by time-reversal if it is invariant for the transformation:

$$q \rightarrow -q, v \rightarrow v, z \rightarrow -z, t \rightarrow -t.$$

It is clear that system (3) shows time-reversal. This concept will be used to apply dissipative KAM theory to system (3). For the general theory see the introductions and statements in [22], [16] and [9].

A second observation is that replacing x, \dot{x} by $-x, -\dot{x}$ keeps the system invariant.

The phase-flow is globally characterised by writing system (3) as a first order ODE in 3-space $\dot{x} = F(x)$ and taking the divergence (*Div*) of the vector field:

$$Div F(x) = -bz. \tag{4}$$

Suppose first that $z(t)$ tends to a fixed non-zero number. If $z(t)$ is positive definite the flow is contracting, if $z(t)$ is negative definite the flow is expanding. In the first case we may find attracting solutions.

The symmetry conditions we have obtained allow in specific phase-space regions solutions with $z(t)$ alternating and in particular $z(t)$ T -periodic. If in the periodic case we have

$$\frac{1}{T} \int_0^T z(t) dt = 0,$$

together with the time-reversal characteristic, dissipative KAM theory will conclude to the existence of invariant tori.

Note that related but different types of control exist in neurodynamics called ‘gating’. An electro-physical signal fires a neuron if it exceeds a potential typical for the gates of the particular neuron. Such a control is different from thermostatic or energy control as in realistic neuron models a potential that is too small will leave the neuron inert. Such neuronal dynamical systems serve however as an inspiration in the present paper. We expect that the study of systems with energy control will also be of use in other biophysical systems.

2.1. Small Oscillations Near the z-Axis, Canards

We scale $q = \sqrt{\epsilon}x, \dot{q} = \sqrt{\epsilon}\dot{x}, a = \epsilon a_0, b = \epsilon b_0$. System (3) becomes:

$$\begin{cases} \ddot{x} + \epsilon b_0 z \dot{x} + x &= -\epsilon c x^3, \\ \dot{z} &= \epsilon(x^2 + \dot{x}^2 - a_0) + O(\epsilon^2), \end{cases} \tag{5}$$

We apply averaging to system (5); see for the theory [23] or [34]. Here and in the sequel we formulate variational equations in amplitude-phase variables r, ϕ . Considering coupled systems of oscillators r, ϕ will be vectors with subscripts r_1, r_2, ϕ_1 etc. Putting $x = r(t) \cos(t + \phi(t)), \dot{x} = -r(t) \sin(t + \phi(t))$ and rescaling produces:

$$\begin{cases} \dot{r} &= -\epsilon \sin(t + \phi)(-cr^3 \cos^3(t + \phi) + b_0 z r \sin(t + \phi)), \\ \dot{\phi} &= -\frac{\epsilon}{r} \cos(t + \phi)(-cr^3 \cos^3(t + \phi) + b_0 z r \sin(t + \phi)), \\ \dot{z} &= \epsilon(r^2 - a_0) + O(\epsilon^2). \end{cases} \tag{6}$$

Averaging over t keeping r, ϕ fixed we find:

$$\dot{r} = -\epsilon \frac{b_0}{2} z r, \dot{\phi} = \epsilon \frac{3}{8} c r^2, \dot{z} = r^2 - a_0. \tag{7}$$

The solutions of system (6) are approximated to $O(\epsilon)$ on an interval of time $O(1/\epsilon)$ by the solutions of system (7).

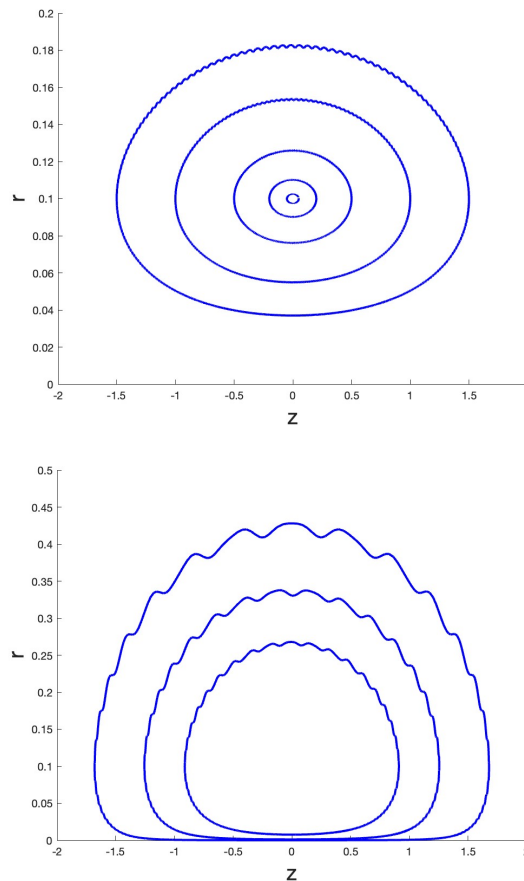


Figure 2. Dynamics near the z -axis based on system (3). Left the closed curves in a r, z -diagram describing the tori around the periodic solution approximated by eq. (7); The initial conditions are $q(0) = 0.1, \dot{q}(0) = 0, z(0) = 0.05, 0.2, 0.5, 1, 1.5$ with parameters $a = 0.01, b = 0.01, c = 1$. Right canard behaviour near the z -axis with initial conditions $q(0) = 0.01, \dot{q}(0) = 0.01, z(0) = 0.5, 1, 1.5$ with parameters $a = 0.01, b = 0.1, c = 1$.

The averaged system (7) contains a periodic approximate solution of the form: 161

$$x(t) = \sqrt{a_0} \cos(t + \varepsilon \frac{3}{8} a_0 t), z(t) = 0. \tag{8}$$

The approximation of the solution of system (5) with initial conditions $x(0) = \sqrt{a_0}, \dot{x}(0) = 0, z(0) = 0$ by expressions (8) has error $O(\varepsilon)$ on the long timescale $1/\varepsilon$. It corresponds with the exact periodic solution obtained with nearby initial conditions. 162
163
164

There is a theoretical advantage giving more insight by using the timelike variable $s = t + \phi$ instead of t ; s is indeed timelike as the phase $\phi(t)$ is varying slowly. Repeating the calculation we have by averaging over s the averaged system: 165
166
167

$$\frac{dr}{ds} = -\varepsilon \frac{b_0}{2} z r, \frac{dz}{ds} = \varepsilon (r^2 - a_0). \tag{9}$$

We have $r = \sqrt{a_0}, z = 0$ as a critical point of the averaged system (9). The determinant in the critical point does not vanish for $a_0 > 0$ so the approximation (8) corresponds with an existing periodic solution of the original system that is 2π -periodic in s . The eigenvalues in the critical point are $\pm i\sqrt{a_0 b_0}$ so the periodic solution is to first approximation neutrally stable. A second order approximation in ε does not change the picture qualitatively as the time-reversibility plays an essential role producing an infinite set of KAM tori, see fig. 2. In 168
169
170
171
172
173

these cases $z(t)$ alternates around $z = 0$. The periodic solution obtained above serves as an organising centre. The solutions $z(t)$ are symmetric with respect to $z = 0$ as predicted. Families of invariant tori were observed earlier for the dissipative Sprott A system in [19]-[20], the mathematical explanation by time-reversal and symmetry was given in [3].

Canards Near the z-Axis

The dynamics near the z-axis as shown in fig. 2 is obtained with parameter $a = O(\varepsilon)$. System (3) was designed to find a periodic solution by averaging close to the z-axis. The system can also be interpreted as a slow-fast system with fast variables q, \dot{q} and slow variable z . According to the theory of slow-fast systems, see [33] and further references there, a slow manifold will be given by $\dot{x} = \dot{x} = 0$ (the z-axis). The slow manifold is not normally hyperbolic so the attraction or repelling is not necessarily exponential but the explicit form makes characterisation easy. If we start with a positive value of $z(0)$ and with $r^2(0) = x^2(0) + \dot{x}^2(0) < a_0$ the solution will move closer to the slow manifold. As long as $z(t) > 0$, $r^2(t)$ will decrease because of dissipation. At time $t = t_1$, $z(t_1) = 0$ and the term $bz\dot{x}$ will produce excitation for $t > t_1$. The slow manifold becomes unstable but as the solutions are very close to the z-axis they will persist for some time in motion near the z-axis; this is the canard phenomenon. The symmetry of the equations causes the jump-off point of the solutions to be mirroring the approach point, see again fig. 2 (right).

2.2. Generalisations

The results obtained thus far for the case $f(q) = cq^3$ and small oscillations carry over to the more general case with $f(q)$ polynomial or analytic, odd and $f(0) = f'(0) = 0$. In particular we have time-reversibility producing invariant tori near the z-axis around a periodic solution as organising centre. Close to the z-axis we will find canard behaviour. In this section we drop the assumption of small oscillations.

A Family of Periodic Solutions

Consider again system (3) with small damping coefficient b and small nonlinear force; put $b = \varepsilon b_0, c = \varepsilon c_0$. System (3) becomes;

$$\begin{cases} \ddot{q} + \varepsilon b_0 z \dot{q} + q + \varepsilon c_0 q^3 &= 0, \\ \dot{z} &= q^2 + \dot{q}^2 + \varepsilon \frac{c_0}{4} q^4 - a, \end{cases} \tag{10}$$

If $\varepsilon = 0$ the solutions for $q(t)$ are harmonic. Transforming system (10) for $\varepsilon \geq 0$ to amplitude-phase variables it becomes a slow-fast system with slow variables r, ϕ and fast variable z :

$$\begin{cases} \dot{r} &= -\varepsilon \sin(t + \phi)((c_0 r^3 \cos^3(t + \phi)) + b_0 z r \sin(t + \phi)), \\ \dot{\phi} &= -\frac{\varepsilon}{r} \cos(t + \phi)(c_0 r^3 \cos^3(t + \phi)) + b_0 z r \sin(t + \phi), \\ \dot{z} &= r^2 - a + O(\varepsilon). \end{cases} \tag{11}$$

We can identify $r = \sqrt{a}$ as a resonance manifold of system (11), for the theory see [33] ch. 12 or [34] ch. 7. Another approach is to use iteration of an integral equation, see [33] ch. 10.2 or [34] ch. 3, this would be an application of the Poincaré-Lindstedt (continuation) method.

Consider a neighbourhood of the resonance manifold by introducing a local variable ξ :

$$\xi = \frac{r - \sqrt{a}}{\delta(\varepsilon)}, \quad r = \sqrt{a} + \delta(\varepsilon)\xi, \tag{12}$$

with $\delta(\varepsilon) = o(1)$ as $\varepsilon \rightarrow 0$. Introducing ζ in system (11) we find:

$$\begin{cases} \delta(\varepsilon)\dot{\zeta} &= -\varepsilon \sin(t + \phi)(c_0(\sqrt{a} + \delta\zeta)^3 \cos^3(t + \phi) + b_0z(\sqrt{a} + \delta\zeta) \sin(t + \phi)), \\ \dot{\phi} &= -\frac{\varepsilon}{(\sqrt{a} + \delta\zeta)} \cos(t + \phi)(c_0(\sqrt{a} + \delta\zeta)^3 \cos^3(t + \phi) + b_0z(\sqrt{a} + \delta\zeta) \sin(t + \phi)), \\ \dot{z} &= (\sqrt{a} + \delta\zeta)^2 - a + O(\varepsilon). \end{cases} \quad (13)$$

A significant degeneration in the sense of singular perturbation theory gives the choice $\delta(\varepsilon) = \sqrt{\varepsilon}$. Expanding while keeping terms $O(\sqrt{\varepsilon})$ we have:

$$\begin{cases} \dot{\zeta} &= -\sqrt{\varepsilon} \sin(t + \phi)(c_0(\sqrt{a} \cos(t + \phi))^3 + b_0z\sqrt{a} \sin(t + \phi)) + O(\varepsilon), \\ \dot{\phi} &= O(\varepsilon), \\ \dot{z} &= 2\sqrt{a\varepsilon}\zeta + O(\varepsilon). \end{cases} \quad (14)$$

Averaging over time produces to $O(\sqrt{\varepsilon})$:

$$\dot{\zeta} = -\sqrt{\varepsilon} \frac{b_0}{2} \sqrt{a} z, \dot{\phi} = 0, \dot{z} = \sqrt{\varepsilon} 2\sqrt{a}\zeta. \quad (15)$$

Consider $t + \phi$ as a timelike variable and the dynamics of the variables ζ, z . The Jacobian of the averaged equations of ζ, z is not singular (its value is $\varepsilon b_0 a$), so according to the implicit function theorem we have existence of the periodic solution continued from the harmonic solution for $\varepsilon = 0$.

Solving the averaged system we find $\zeta^2 + \frac{b_0}{4} z^2 = \text{constant}$ corresponding with neutral stability for critical point $\zeta = z = 0$ in the resonance manifold. However, a first order approximation in a resonance manifold will always yield conservative dynamics even if the original system is dissipative; see for the general theory again [33] ch. 12 or [34] ch. 7. So we have to construct a second order approximation to establish stability.

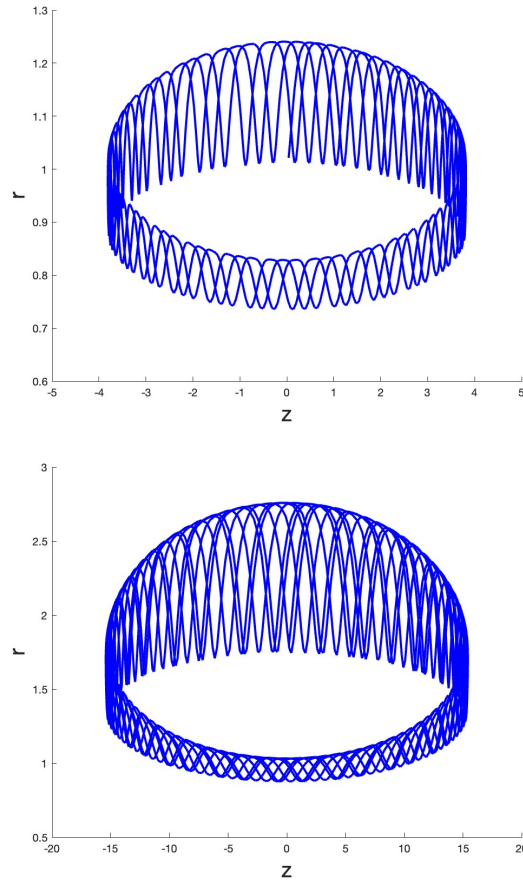


Figure 3. Dynamics based on system (3). for 2 cases starting close to $r = \sqrt{a}, z = 0$. with $a = 1, 3$ and parameters $b = 0.01, c = 1$. In both cases a torus emerges around $r = \sqrt{a}$.

Expansion to $O(\varepsilon)$ leads to the system:

223

$$\begin{cases} \dot{\zeta} &= -\sqrt{\varepsilon} \sin((t + \phi))[-a^{3/2} \cos^3(t + \phi) + b_0 \sqrt{a} z \sin(t + \phi)] \\ &\quad -\varepsilon \sin(t + \phi)[-3a\zeta \cos^3(t + \phi) + b_0 z \zeta \sin(t + \phi)] + \varepsilon^{3/2}, \\ \dot{\phi} &= -\varepsilon \cos(t + \phi)[-a \cos^3(t + \phi) + b_0 z \sin(t + \phi)] + \varepsilon^{3/2}, \\ \dot{z} &= \sqrt{\varepsilon} 2\sqrt{a} \zeta + \varepsilon \zeta^2. \end{cases} \tag{16}$$

However the second order averaging (see [33] or [34]) the system (13) does not change the neutral stability.

224

225

Numerical explorations for $a = 1, 2, 4, 9$ and nearby initial conditions show instability of $\zeta = z = 0$ and convergence to other solutions. See fig. 3 for the cases of orbits starting near $a = 1, z = 0$ and $a = 2, z = 0$.

226

227

228

3. A Coupled System of 2 Controlled Oscillators

We extend system (3) to two coupled systems with a simple direct coupling. The coupling is not inspired by pendulum couplings but by the process of transmitting impulses to neighbouring components as in neural systems. Consider the coupled system:

$$\begin{cases} \dot{q}_1 + bz_1\dot{q}_1 + q_1 + cq_1^3 &= \beta q_2, \\ \dot{z}_1 &= q_1^2 + \dot{q}_1^2 + \frac{c}{4}q_1^4 - a_1, \\ \dot{q}_2 + bz_2\dot{q}_2 + q_2 + cq_2^3 &= \beta q_1, \\ \dot{z}_2 &= q_2^2 + \dot{q}_2^2 + \frac{c}{4}q_2^4 - a_2. \end{cases} \tag{17}$$

The interaction constant $\beta \geq 0$ will determine the interaction force. In system (17) the first component activates the second, the second one the first. We assume $a_1, a_2 > 0$.

The result of lemma 1 extends in the following form:

Lemma 2. *If $b = \beta = 0$ the corresponding solutions $q_1(t), q_2(t)$ of system (17) are quasi-periodic, they are periodic if the initial conditions are equal.*

As we shall see, system (17) will produce for $\beta > 0$ interactions of quasi-periodic oscillations with complicated dynamics. In [14] and [27] such two-frequency interactions are studied involving torus bifurcations and chaotic dynamics characterised by Lyapunov-exponents. The nature of the coupling in [14] and [27] is different from our system (17) with more complicated dissipation. A common feature is that in both model systems a form of self-excitation takes place.

System (17) can be written as a first order system $\dot{x} = F(x)$ in 6-space with divergence:

$$Div F(x) = -b(z_1 + z_2). \tag{18}$$

So, in a region where $z_1 + z_2 > 0$, the flow contracts, if in the region $z_1 + z_2 < 0$, the flow expands.

Lemma 3. *If $c = \beta = 0$ in system (17) we have a family of harmonic synchronised periodic solutions in the manifold $z_1 = z_2 = 0$ of the form:*

$$q_1(t) = \sqrt{a_1} \cos t, \dot{q}_1(t) = -\sqrt{a_1} \sin t, q_2(t) = \sqrt{a_2} \cos t, \dot{q}_2(t) = -\sqrt{a_2} \sin t. \tag{19}$$

If $\beta \neq 0$ we expect instability of the periodic solution because of resonance. It is natural to study the cases $c, \beta \ll 1$.

3.1. Small Interactions and Small Oscillations

Consider the case of small interactions $\beta = \epsilon\beta_0$, small deflections and consequently small nonlinearity cq^3 ; put $b = \epsilon b_0$.

As in subsection 2.1 we can scale for the deflections $q_{1,2} = \sqrt{\epsilon}x_{1,2}$, for the velocities $\dot{q}_{1,2} = \sqrt{\epsilon}\dot{x}_{1,2}$, $a_{1,2} \rightarrow \epsilon a_{1,2}$. Introducing amplitude-phase coordinates as before and by averaging as in subsection 2.1 we find the system for $O(\epsilon)$ approximations given by:

$$\begin{cases} \dot{r}_1 &= -\epsilon(r_1 \frac{b_0}{2} z_1 + \frac{\beta_0}{2} r_2 \sin(\phi_1 - \phi_2)), \phi_1 = \epsilon(\frac{3}{8}cr_1^2 - \frac{\beta_0 r_2}{2r_1} \cos(\phi_1 - \phi_2)), \\ \dot{r}_2 &= -\epsilon(r_2 \frac{b_0}{2} z_2 + \frac{\beta_0}{2} r_1 \sin(\phi_2 - \phi_1)), \phi_2 = \epsilon(\frac{3}{8}cr_2^2 - \frac{\beta_0 r_1}{2r_2} \cos(\phi_2 - \phi_1)), \\ \dot{z}_1 &= \epsilon(r_1^2 - a_1) + O(\epsilon^2), \dot{z}_2 = \epsilon(r_2^2 - a_2) + O(\epsilon^2). \end{cases} \tag{20}$$

Structurally stable critical points of the approximating vector field correspond with periodic solutions close to the critical points, see [34].

We have the critical values $r_1 = \sqrt{a_1}, r_2 = \sqrt{a_2}$. Put for the combination angle $\chi = \phi_1 - \phi_2$. The equation for χ becomes:

$$\frac{d\chi}{dt} = \frac{\varepsilon}{2} \left[\frac{3}{4}c(r_1^2 - r_2^2) - \beta_0 \left(\frac{r_2}{r_1} - \frac{r_1}{r_2} \right) \cos \chi \right]. \tag{21}$$

The case $a_1 = a_2 = a$

This is clearly a degenerate case as from (21) we have in the critical points $r_1 = r_2$ and so $d\chi/dt = 0$. The only requirement is $z_1 = -z_2$ but with χ not determined. The timeseries $q_1(t), q_2(t)$ corresponding to the critical points are shown in fig. 4. As expected from the analysis of 1 component in section 2, see also fig. 2, the canard behaviour becomes less prominent when decreasing $z_1(0), z_2(0)$. This is illustrated in figs. 4 and 5 where $a_1 = a_2 = 0.0025$. Choosing $z_1(0) = 2, z_2(0) = -2$ we have canard behaviour, decreasing the initial z -values we find the irregular pattern shown in fig. 6 for $q_1(t)$ (and the same for $q_2(t)$). The irregularity originates from the exponential closeness of the orbits to the slow manifold at the z -axis which is not normally hyperbolic.

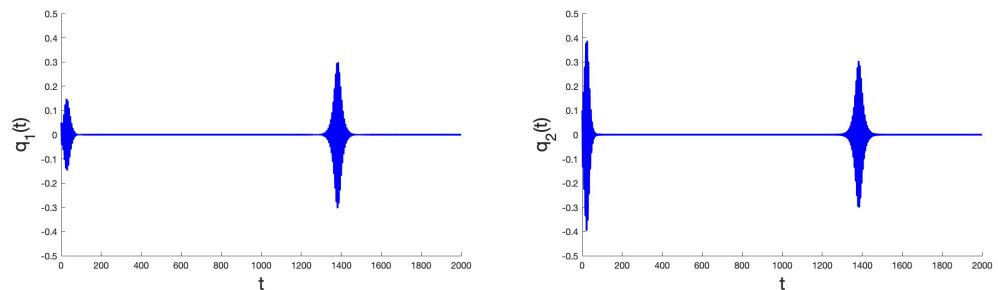


Figure 4. Consider the critical point of system (20) $q_1 = q_2 = 0.05, \dot{q}_1 = \dot{q}_2 = 0, z_1 = 0.2, z_2 = -0.2$ and parameters $a_1 = a_2 = 0.0025, b = 0.1, c = 1, \beta = 0.1$. The timeseries of the corresponding periodic solution shows spiking caused by canard behaviour.

Starting close to the critical point the dynamics shows instability. See fig. 5 for an example, the numerics based on system (17) suggests the presence of a torus.

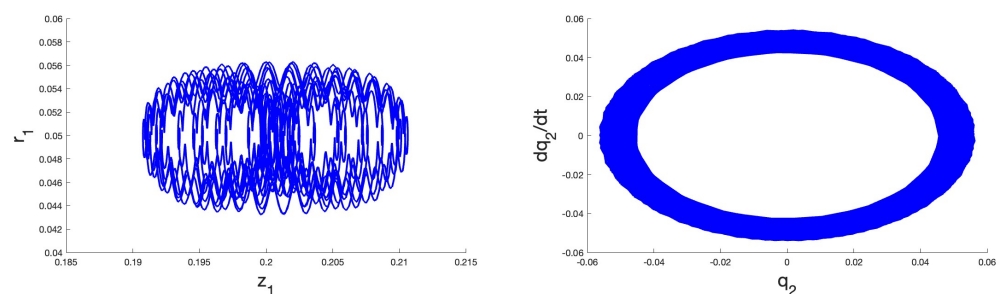


Figure 5. Dynamics for small oscillations based on system (17). Left the r_1, z_1 -diagram and right the q_2, \dot{q}_2 -diagram describing the projected tori around the periodic solution. The initial conditions are $q_1(0) = 0.0501, \dot{q}_1(0) = 0.0001, z_1(0) = 0.2, q_2 = 0.0499, \dot{q}_2 = -0.0001, z_2 = -0.21$ with parameters $a_1 = a_2 = 0.0025, b = 0.1, c = 1, \beta = 0.1$.

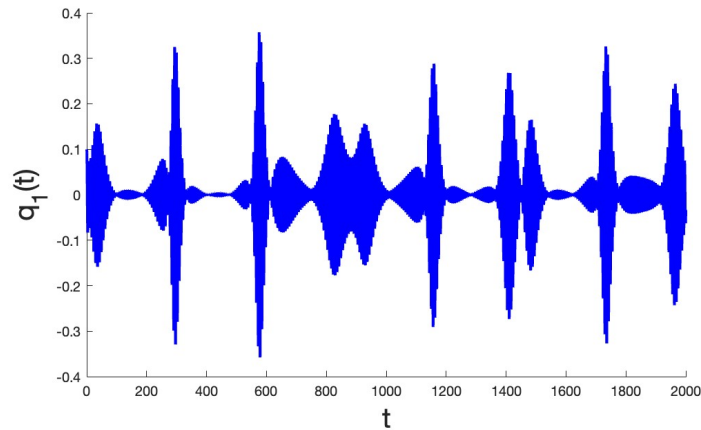


Figure 6. Consider the critical point $q_1 = q_2 = 0.1, \dot{q}_1 = \dot{q}_2 = 0, z_1 = 1.3, z_2 = -1.3$ and parameters $a_1 = a_2 = 0.01, b = 0.1, c = 1, \beta = 0.1$. The timeseries shows the case with for these initial z -values the transition to canard behaviour.

The case $a_1 \neq a_2$

This case yields as well nontrivial equilibria. Requiring $\dot{\chi} = 0$ gives the following condition.

$$\cos \chi = -\frac{3c\sqrt{a_1 a_2}}{4\beta_0} \tag{22}$$

Note that equation (22) implies that $|3c\sqrt{a_1 a_2}/(4\beta_0)| \leq 1$. Looking for roots of the amplitude equations yields:

$$\begin{cases} \sin \chi = -\frac{\sqrt{a_1} b_0 z_1}{\sqrt{a_2} \beta_0} \\ \sin \chi = \frac{\sqrt{a_2} b_0 z_2}{\sqrt{a_1} \beta_0} \end{cases} \tag{23}$$

This gives the two nontrivial equilibria solutions in the case $a_1 \neq a_2$.

$$\begin{aligned} r_1 &= \sqrt{a_1}, r_2 = \sqrt{a_2}, \\ z_2 &= -\frac{a_1}{a_2} z_1, \end{aligned} \tag{24}$$

$$z_1 = \pm \sqrt{\frac{16a_2\beta_0^2 - 9c^2a_1a_2^2}{16a_1b_0^2}}, \tag{25}$$

$$\chi = \pi + \arctan\left(\frac{4b_0z_1}{3ca_2}\right), \quad \text{if } \beta_0c > 0, \tag{26}$$

$$\chi = \arctan\left(\frac{4b_0z_1}{3ca_2}\right), \quad \text{if } \beta_0c \leq 0 \tag{27}$$

The Jacobian matrix of system (20) at the nontrivial equilibrium in the case $a_1 \neq a_2$ and small oscillations is as follows:

$$DF(x) = \begin{pmatrix} -\frac{bz_1}{2} & \frac{3}{8}ca_2\sqrt{a_1} & \frac{\sqrt{a_1}bz_1}{2\sqrt{a_2}} & -\frac{\sqrt{a_1}b}{2} & 0 \\ \frac{3c(a_1-a_2)}{8\sqrt{a_1}} & \frac{bz_1(a_1-a_2)}{2a_2} & \frac{3c(a_1-a_2)}{8\sqrt{a_2}} & 0 & 0 \\ -\frac{\sqrt{a_1}bz_1}{2\sqrt{a_2}} & -\frac{3}{8}ca_1\sqrt{a_2} & \frac{a_1bz_1}{2a_2} & 0 & -\frac{\sqrt{a_2}b}{2} \\ 2\sqrt{a_1} & 0 & 0 & 0 & 0 \\ 0 & 0 & 2\sqrt{a_2} & 0 & 0 \end{pmatrix} \tag{28}$$

The trace of the Jacobian (28) is

$$Tr(DF) = bz_1 \frac{a_1 - a_2}{a_2}. \tag{29}$$

The trace vanishes to produce degenerate dynamics in the 2 cases:

$$a_1 = a_2, 16\beta_0^2 = 9c^2 a_1 a_2. \tag{30}$$

In the second case we have $z_1 = z_2 = 0$, see again fig. 5.

An analysis of the eigenvalues of the nontrivial equilibria for the case $a_1 \neq a_2$ reveals that the equilibria are of unstable focus type. For the parameter values $a_1 = 0.25, a_2 = 0.15, b = 1, \beta = 1, c = 1, \epsilon = 1$, we identify two nontrivial equilibria with $z_1 = \pm 0.766384$ and corresponding eigenvalues:

$$\Lambda_1 = \{-0.0495 \pm 0.5553i, 0.1838 \pm 0.3056i, 0.2423\}, \tag{31}$$

$$\Lambda_2 = \{0.0495 \pm 0.5553i, -0.1838 \pm 0.3056i, 0.2423\}. \tag{32}$$

Further continuation of the equilibria with respect to the system's parameters does not reveal any significant bifurcations.

3.1.1. Quasi-Periodic Motion and Associated Bifurcations

Interestingly, the averaged system (20) contains in the case $a_1 \neq a_2$, a stable periodic orbit, unrelated to the equilibria mentioned so far. This implies the presence in the original system of quasi-periodic motion in the form of a stable two-dimensional torus that can be depicted numerically starting in the neighborhood of the averaged stable cycle, see fig. 7 and for the Lyapunov-exponents fig. 8. A more general discussion explaining why we find 2 Lyapunov-exponents zero is presented in appendix A.

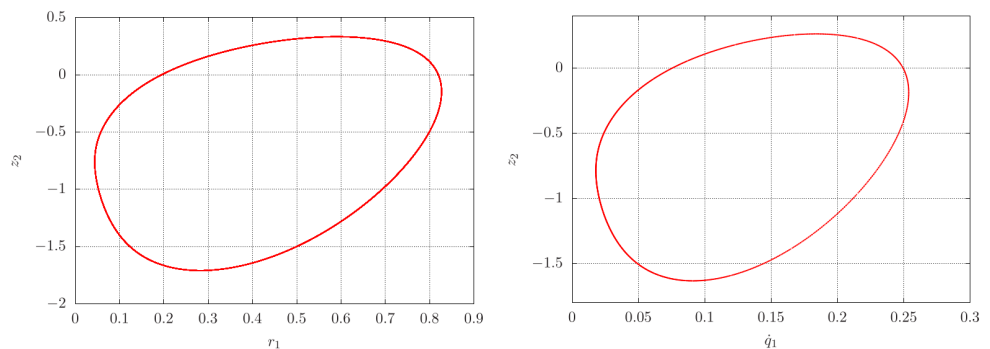


Figure 7. Left: A stable cycle, with period $T = 13.7288$, numerically obtained from the averaged system (20) with initial condition: $r_1 = 0.0518, \chi = 4.273, r_2 = 0.099, z_1 = 1.119, z_2 = -0.989$, and parameters $a_{01} = 0.15, a_{02} = 0.25, b_0 = \beta_0 = c = 1, \epsilon = 0.1, a_1 = \epsilon a_{01}, a_2 = \epsilon a_{02}$. Right: Poincaré section ($q_1 = 0$) of system (17) projected onto the (\hat{q}_1, z_2) -plane with initial condition: $q_1 = 0; \hat{q}_1 = 0.1276, q_2 = 0.216, \hat{q}_2 = 0.006, z_1 = 0.638, z_2 = -1.569$, and parameters $a_1 = 0.015, a_2 = 0.025, b = \beta = 0.1, c = 1$, showing a closed curve corresponding with a two-dimensional torus.

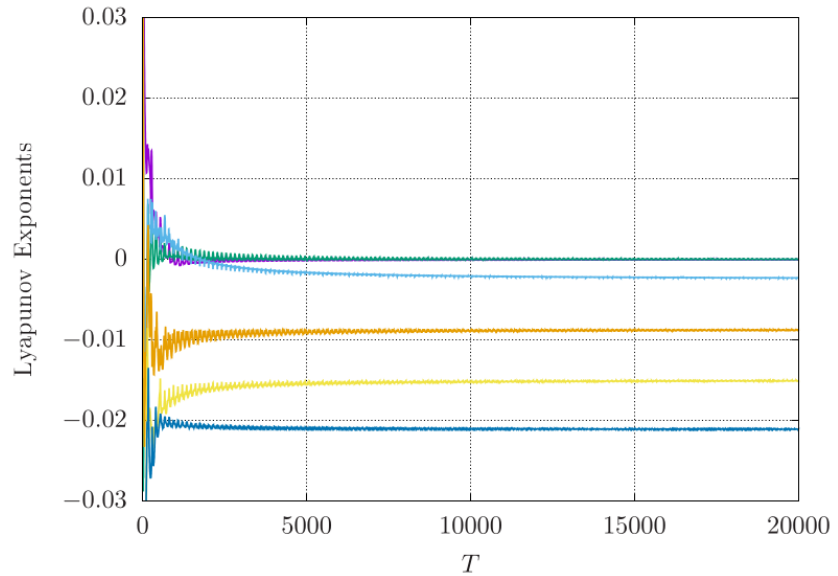


Figure 8. Lyapunov exponents of the stable single torus (Figure 7, right), showing two zero exponents and four negative exponents.

Continuation of the limit cycle in the averaged system using a_2 as a control parameter reveals a supercritical period-doubling at the critical value $a_2 = 0.2285909$ from which a stable cycle with double the period ($T = 27.9445$) emerges. The corresponding stable double torus in the original system has been numerically located near the double cycle as expected. See Fig. 9.

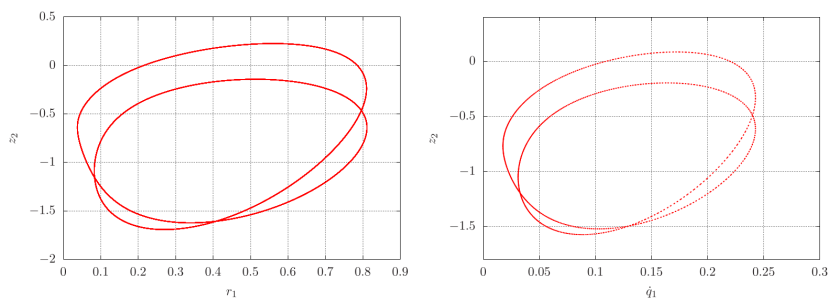


Figure 9. Left: A stable double cycle projected on the r_1, z_2 plane, with period $T = 29.9$, numerically obtained from the averaged system (20) by continuation of the stable period 1 cycle. Right: Poincaré section ($q_1 = 0$) of system (17) projected onto the (\dot{q}_1, z_2) –plane with initial condition: $q_1 = 0; \dot{q}_1 = 0.1742, q_2 = 0.1382, \dot{q}_2 = -0.0426, z_1 = 1.5878, z_2 = 0.0859$, and parameters $a_1 = 0.015, a_2 = 0.02, b = \beta = 0.1, c = 1$, showing a closed curve corresponding with a two-dimensional double torus.

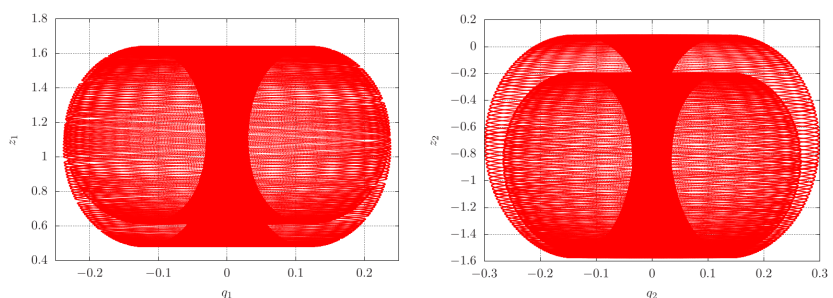


Figure 10. Orbits starting from the same initial conditions as in Figure 7 (right), projected onto the (q_1, z_1) –plane (left) and the (q_2, z_2) –plane (right), illustrating the double torus.

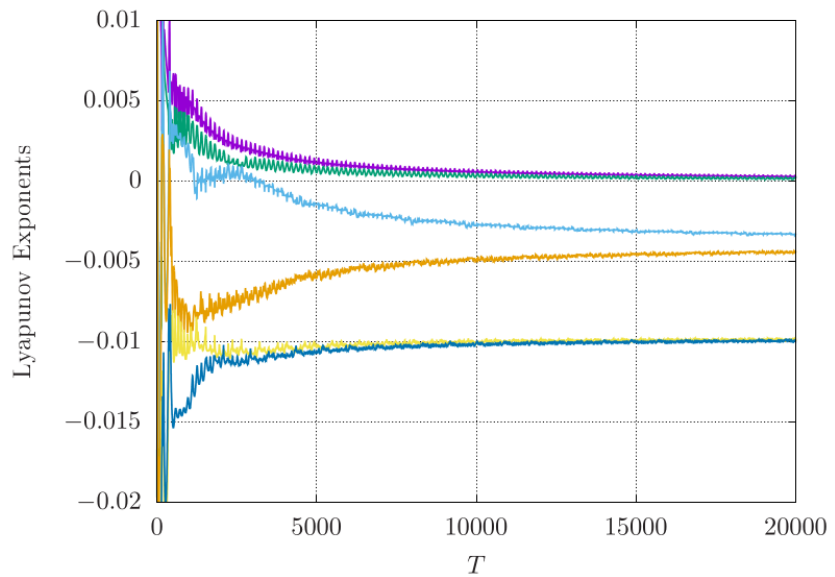


Figure 11. Lyapunov exponents of the stable double torus, as depicted in Figure 9 (Right), showing two zero exponents and the four negative exponents .

3.1.2. Chaos Through the Cascade of Period Doubling in Tori

305

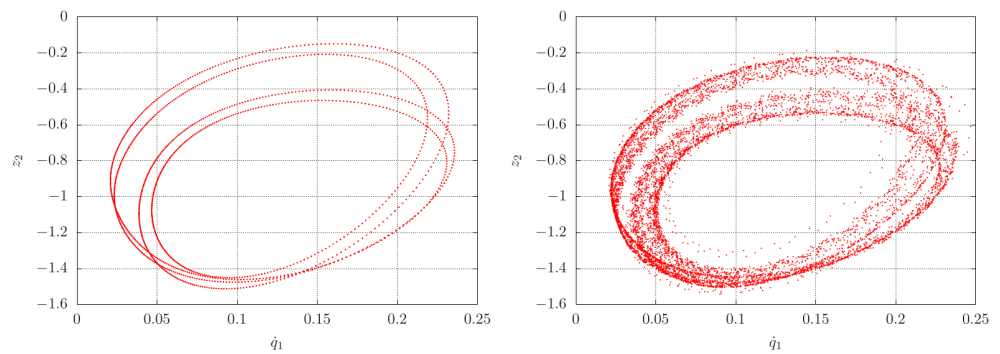


Figure 12. Poincaré section $a_2 = 0.017$ (left) and $a_2 = 0.016$ (right)

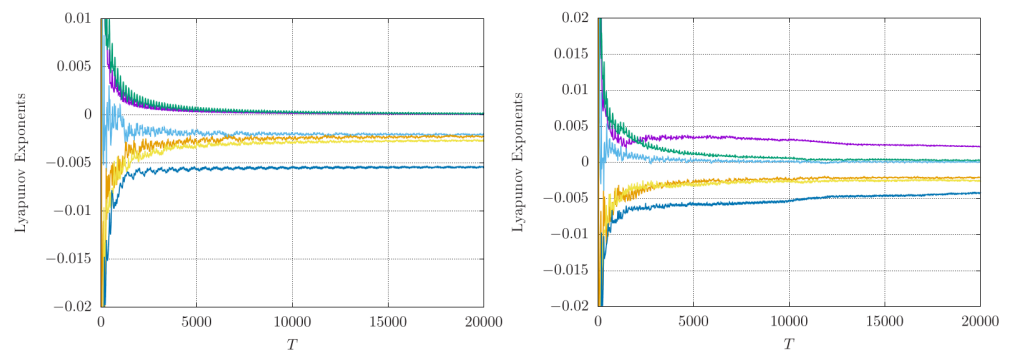


Figure 13. Left: Lyapunov exponents of the stable double torus, $a_2 = 0.017$, with two exponents equal to zero and the remaining four exponents negative. Right: Lyapunov exponents of the strange attractor after the cascade of period doubling at $a_2 = 0.016$ with one positive exponent, two zero exponents and the remaining three negative.

3.1.3. Coexisting Period 2 Orbit

306

Tracking periodic orbits and analyzing their stability through continuation methods is crucial for detecting bifurcations and understanding the resulting dynamics, as well as the routes to chaos in the system under investigation. Using the numerical methods outlined

307

308

309

in [24], an additional period-2 orbit was identified in the averaged system, which coexists with the period-1 cycle shown in Figure 7. This cycle has four complex multipliers on the unit circle and one real multiplier equal to 1. Because the cycle is only Lyapunov stable, there is no guarantee that the corresponding two-dimensional torus exists in the original system. See Figure 14.

310
311
312
313
314

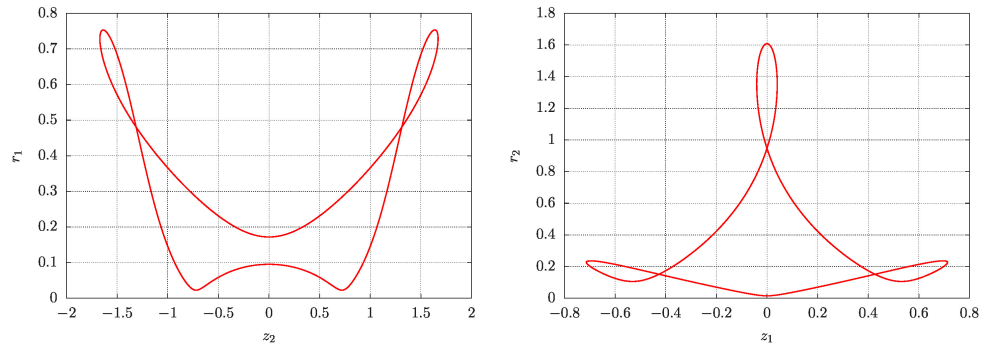


Figure 14. Left: A numerically computed period-2 cycle with period $T = 18.23$ from the averaged system (20), projected onto the z_2 - r_1 plane. The initial conditions are $r_1 = 0.3$, $\chi = 3.94203$, $r_2 = 1.47846$, $z_1 = -0.03541$, and $z_2 = 0.77940$, with parameters $a_{01} = 0.15$, $a_{02} = 0.25$, $b_0 = \beta_0 = c = 1$. Right: The same period-2 cycle, now projected onto the z_1 - r_2 plane, illustrating its behavior across different coordinate projections. The cycle has four complex multipliers on the unit circle and one real multiplier equal to 1.

Searching for the corresponding dynamics in the original system, starting near the Lyapunov stable cycle of the averaged system, the following invariant set was identified. See Figure 15.

315
316
317

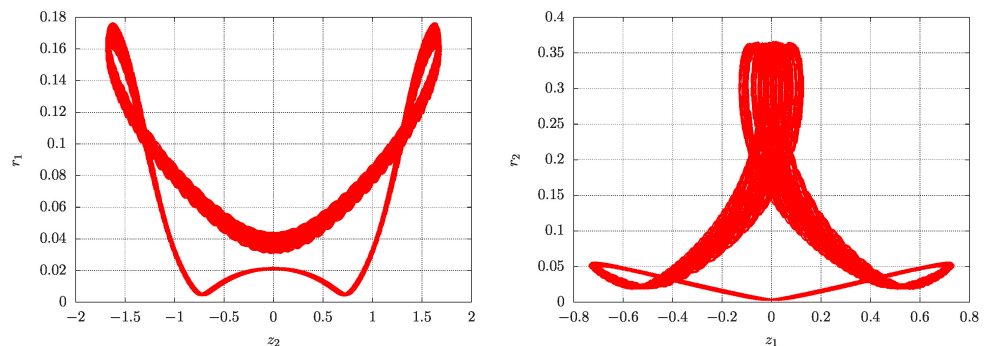


Figure 15. Left: Orbit numerically computed from the original system (17), initiated near the stable cycle, projected onto the z_2 - r_1 plane. The initial conditions are $q_1 = 0$, $\dot{q}_1 = 0.1610127$, $q_2 = 0.00894116$, $\dot{q}_2 = -0.02264744804$, $z_1 = -0.5138185$, and $z_2 = -1.489323$, with parameters $\varepsilon = 0.05$, $a_1 = 0.15\varepsilon$, $a_2 = 0.25\varepsilon$, $b = \beta = \varepsilon$, $c = 1$. Right: The same period-2 orbit, now projected onto the z_1 - r_2 plane, highlighting its behavior across different coordinate projections.

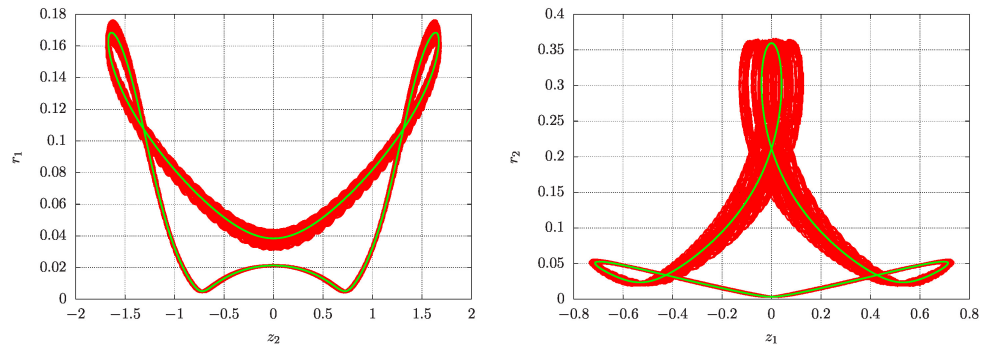


Figure 16. Left: The orbit (in red) numerically computed from the original system (17), initialized near the stable cycle, along with the scaled stable cycle (in green) from the averaged system (20), projected onto the z_2 - r_1 plane. Right: The same orbits, now projected onto the z_1 - r_2 plane, demonstrating the accuracy of the averaging method.

By searching for period-1 and period-2 periodic orbits in the averaged system with initial values $r_1 = 0.3$, $\chi = 0$, r_2 within the interval $(0, 6]$, and z_1, z_2 ranging from -3 to 3 in increments of $1/50$, eight additional periodic orbits were identified that coexist with the two cycles previously found. Four stable and four unstable. See illustrations in Fig. 17.

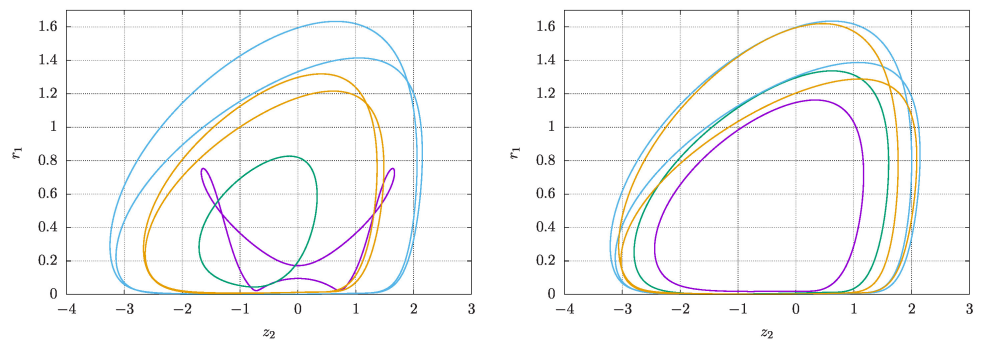


Figure 17. Numerically computed stable periodic orbits of the averaged system, obtained via the fixed point method applied to a Poincaré section. The orbits are projected onto the z_2 - r_1 plane with parameters $\epsilon = 0.05$, $a_{01} = 0.15$, $a_{02} = 0.25$, $b_0 = \beta_0 = c = 1$. Right: Corresponding unstable periodic orbits under the same parameter settings.

3.1.4. Interactions Involving Canards

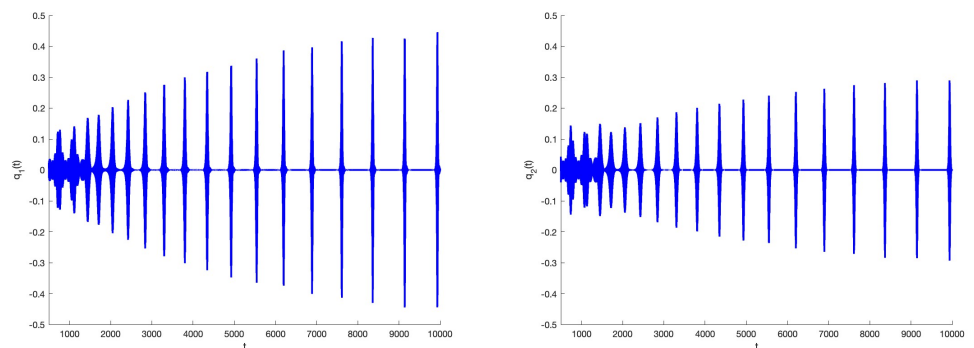


Figure 18. $q_1(t)$ (left) and $q_2(t)$ (right) in the case $a_1 = 0.005$, $a_2 = 0.0025$, $b = 0.1$, $c = 1$, $\beta = 0.1$ and initial conditions $q_1(0) = \sqrt{a_1}$, $q_2(0) = \sqrt{a_2}$, $v_1 = v_2 = 0$, $z_1(0) = 0.5$, $z_2(0) = -1$. The system evolves to canard behaviour with divergence (18) alternating in sign.

318
319
320
321

322

In fig. 18 the evolution of the 2-particle system tends to canard behaviour. The dynamical evolution starts to stabilise after 15000 timesteps. The canard character of the flow is shown in fig. 19 where the projected dynamics suggests a flattened torus; the variable $z_1(t)$ takes negative and positive values, $z_2(t)$ mostly positive ones producing both attraction and repelling.

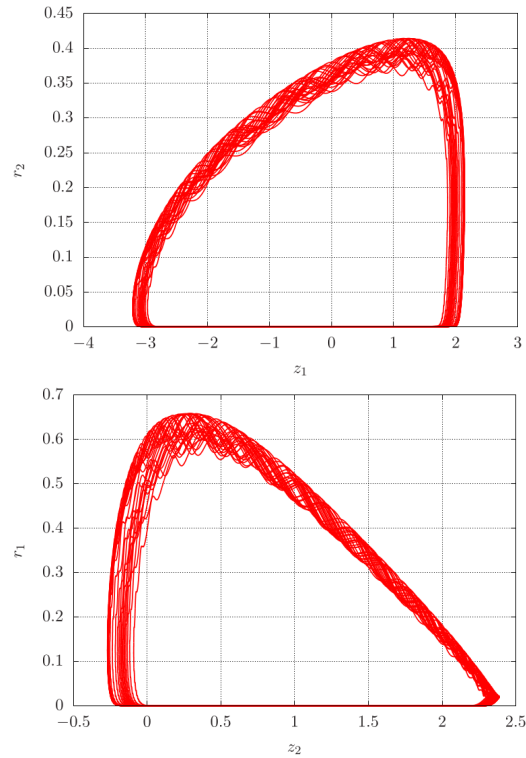


Figure 19. Projections z_1, r_2 (left) and z_2, r_1 (right) in the case of fig. 18. The initial transients are left out by omitting the output of the first 20 000 timesteps. The divergence (18) shows both attraction and repelling.

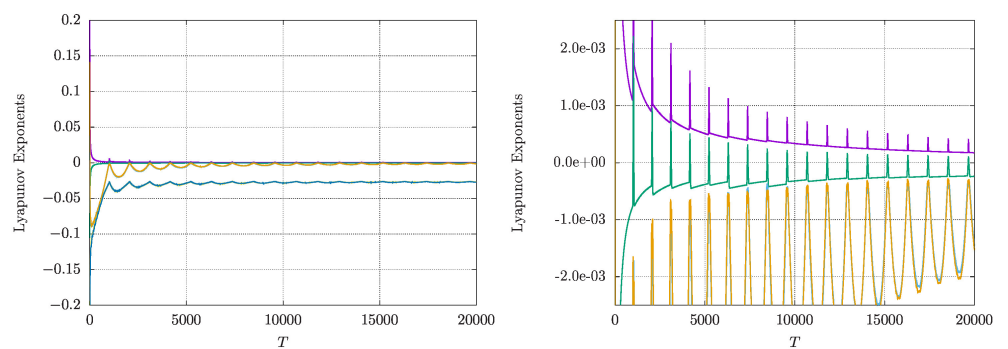


Figure 20. Left: Lyapunov exponents of the flattened torus from Figure 19, illustrating two negative exponents and four exponents clustered near zero. Right: A magnified view of the left figure, highlighting the spiky behaviour of the four Lyapunov exponents close to zero.

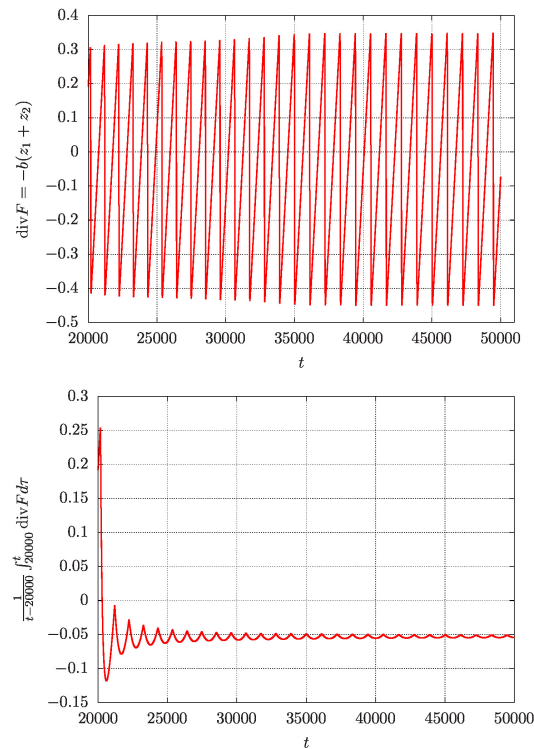


Figure 21. Divergence of the flow of fig. 19 for $t > 20\,000$. Right the average of the divergence (18) tending to a small negative value.

The Lyapunov exponents of the flow shown in fig. 19 have 4 exponents clustered near zero. In fig. 20 right we present an enlarged picture of the small exponents. We find both positive and negative spiky behaviour suggesting small fractal structure of the flattened torus of fig 19. Additional information is shown in fig 21 where we show the alternating divergence of the flow corresponding with alternating attraction and repelling.

3.2. Interactions of Larger Quasi-Periodic Solutions

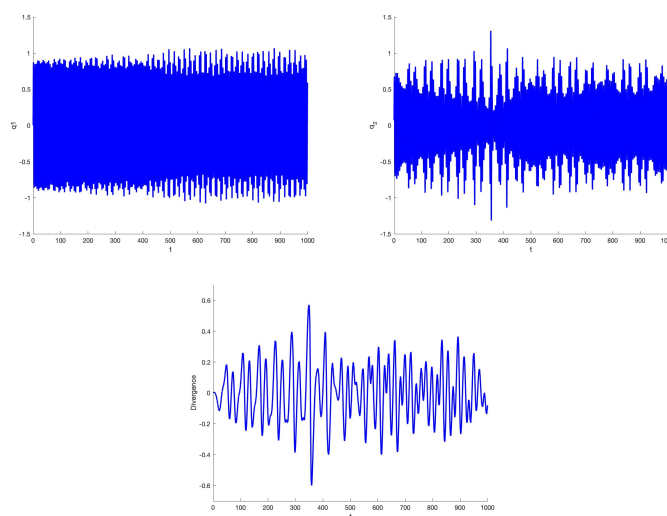


Figure 22. Time-series of 2 quasi-periodic oscillations based on eq. (17) with $q_1 = q_2 = 0, z_1 = z_2 = 0$ and $v_1 = 1, v_2 = \sqrt{0.5}$ with parameters $a_1 = 1, a_2 = 0.5, b = 0.1, c = 1, \beta = 0.1$. Left $q_1(t)$, middle $q_2(t)$ and right the strongly fluctuating divergence of the flow.

Consider the dynamics when leaving the region of small oscillations. In the case of friction parameter b and interaction parameter β still small we consider with $a_1 \neq a_2$ interactions of quasi-periodic solutions. Putting $O(1)$ initial conditions for the coordinates and parameters a_1, a_2 we obtain chaotic solutions, see fig. 22 where we have chosen $b = \beta = 0.1$. The Lyapunov-exponents for the case $a_1 = 1, a_2 = 0.5$ are depicted in fig. 23. As usual $c = 1$, varying c changes the dynamics but keeps chaos. The exponents are: $\lambda_1 = 0.86164049916299E - 02; \lambda_2 = 0.28784389624742E - 02; \lambda_3 = 0.33455860114490E - 03; \lambda_4 = -0.14209055102249E - 03; \lambda_5 = -0.24875434928298E - 02, \lambda_6 = -0.10024345648336E - 01$. The dynamics turns out to be hyper-chaotic with 2 positive exponents.

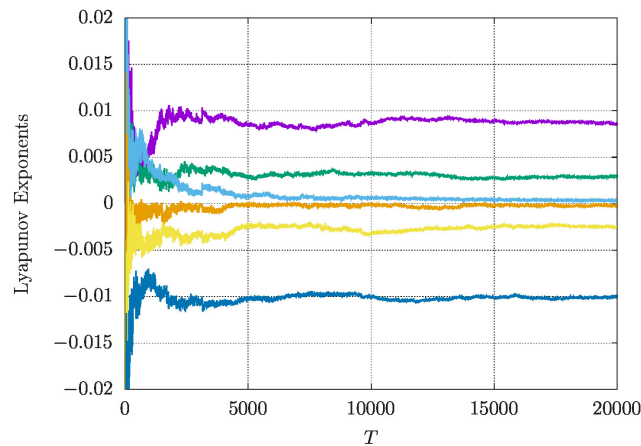


Figure 23. Interactions of 2 quasi-periodic oscillations based on eq. (17) with initially $q_1 = q_2 = 0, z_1 = z_2 = 0$ and $v_1 = 1, v_2 = \sqrt{0.5}$ with parameters $a_1 = 1, a_2 = 0.5, b = 0.1, c = 1, \beta = 0.1$.

Larger Interaction Parameter β

Exploring systematically the case of $O(1)$ values of β we find tori, chaos and hyper-chaos. The hyperchaos found in the system of fig. 23 associated with 2 L- exponents is investigated with other phenomena for the values of b, β between 0 and 1, see fig. 24. We find small islands (yellow) in a sea of chaotic cases (green). The chaotic cases are associated with one L-exponent. In a neighbourhood of $b = \beta = 0$ we find 2-dimensional tori blue as found earlier for the case of small interactions and small oscillations, but interestingly we have also for small dissipation sets of chaotic solutions. The picture of phenomena of many cases in fig. 24 is very remarkable and not easy to predict analytically.

Consider again system (17). Assume that $0 < \beta < 1, b = \epsilon b_0, c = \epsilon c_0$. To study the emergence of tori for forced 2-frequency oscillations consider the system:

$$\begin{cases} \dot{q}_1 + \epsilon b_0 z_1 q_1 + q_1 + \epsilon c_0 q_1^3 &= \beta q_2, \\ z_1 &= q_1^2 + \dot{q}_1^2 + \epsilon \frac{c_0}{4} q_1^4 - a_1, \\ \dot{q}_2 + \epsilon b_0 z_2 q_2 + q_2 + \epsilon c_0 q_2^3 &= \beta q_1, \\ z_2 &= q_2^2 + \dot{q}_2^2 + \epsilon \frac{c_0}{4} q_2^4 - a_2. \end{cases} \tag{33}$$

For $\epsilon = 0$ we have the quasi-periodic solutions:

$$\begin{cases} q_1 &= r_1 \cos(\sqrt{1 + \beta}t + \phi_1) + r_2 \cos(\sqrt{1 - \beta}t + \phi_2), \\ q_2 &= -r_1 \cos(\sqrt{1 + \beta}t + \phi_1) + r_2 \cos(\sqrt{1 - \beta}t + \phi_2), \end{cases} \tag{34}$$

with r_1, r_2, ϕ_1, ϕ_2 constants determined by the initial conditions. The interactions of these quasi-periodic solutions are shown for small values of b in fig. 25.

357
358

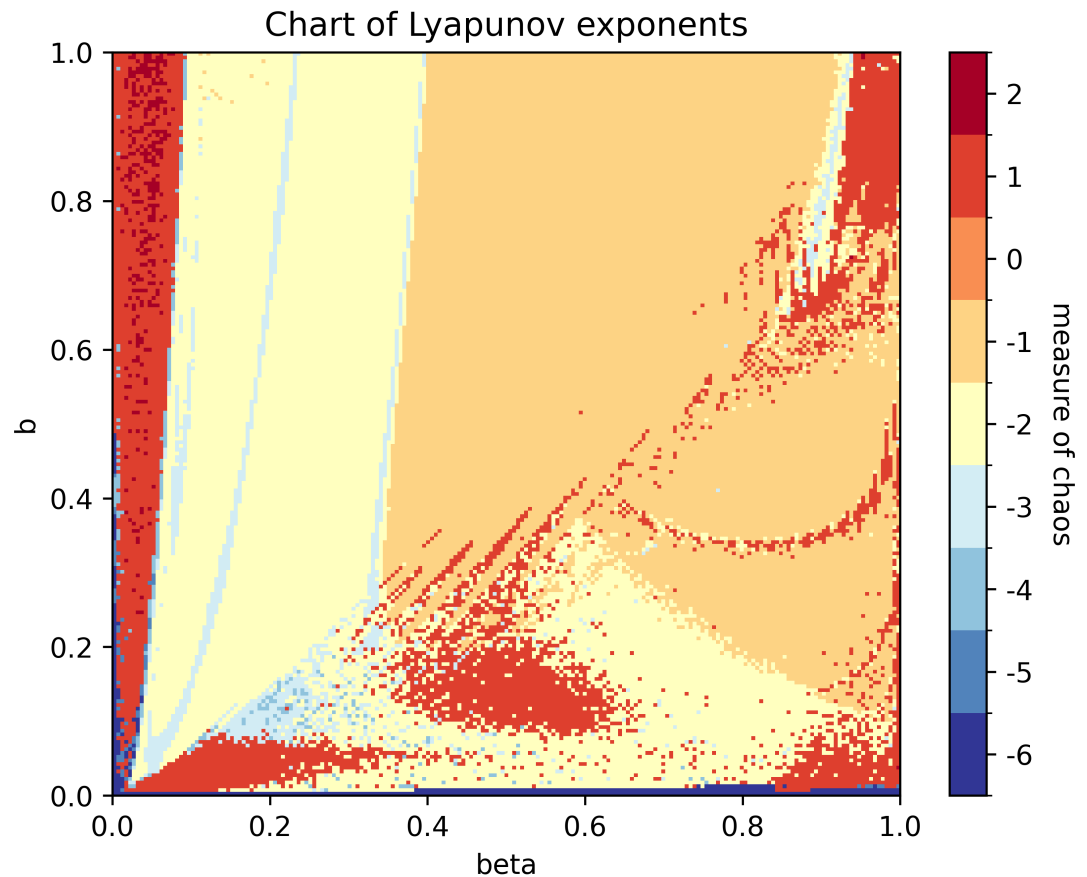


Figure 24. Chart of parameters b, β characterising interactions of 2 quasi-periodic oscillations based on eq. (17), $0 \leq b, \beta \leq 1$, $a_1 = 0.015, a_2 = 0.025, c = 1$. The initial conditions are: $q_1 = 0, v_1 = 0.06955254625606, q_2 = 0.03492489869658, v_2 = -0.02743019598001, z_1 = 1.66213345371198,$ and $z_2 = -0.03710401127306$. The coloring scheme used corresponds to a classification based on the number of zero Lyapunov exponents, with a threshold of 10^{-3} : any exponent with absolute value below this threshold is treated as zero. The values of the exponents, ranging from -6 to 2, are mapped to the *RdYlBu_r* colormap as follows: dark blue regions indicate the absence of clear dynamics, with all six Lyapunov exponents near zero (undecided behavior). Medium-dark blue corresponds to five exponents near zero, indicating a 5D torus, while medium blue (four near-zero exponents) corresponds to a 4D torus, and so on, with light blue corresponding to a 3D torus and yellow to a 2D torus, indicative of quasi-periodic behavior. Orange regions correspond to systems with one zero exponent, representing periodic orbits, while regions in red and dark red indicate chaotic or hyperchaotic dynamics, with one or two positive Lyapunov exponents. For the calculation of the Lyapunov coefficients, integration was performed from $t = 0$ to t_{\max} with a maximum time $t_{\max} = 1.5 \times 10^6$, and the expansion rates were calculated every 100 steps, resulting in 15,000 time steps used to compute the exponents. The integration was carried out using a 4th-order Runge-Kutta (RK4) scheme with step size 10^{-2} .

If $\varepsilon = 0$, the expressions of system (34) with amplitudes and phases constant are general quasi-periodic solutions of system (33). They describe for $0 < \beta < 1$ tori in phase-space. We are interested in the bifurcations arising for $0 < \varepsilon \ll 1$. In fig. 24 we characterise these bifurcations by the Lyapunov-exponents. We find periodic orbits (orange), 2- and 3-tori (resp. yellow and light blue), chaos (red) and hyperchaos (dark red spots).

359
360
361
362
363

The chart uses colors to represent the different dynamics based on the Lyapunov-exponents of the system with the following cases:

- 0: All Lyapunov-exponents are negative (no zeros). This indicates the system settles to an equilibrium state.
- 1: One Lyapunov-exponent is positive. This signifies the presence of chaos in the system.
- 2: Two Lyapunov-exponents are positive. This corresponds to hyperchaos, where the system exhibits even more complex behavior.
- -1: One Lyapunov-exponent is zero, and all others are negative. This reflects a periodic orbit.
- -2: Two Lyapunov-exponents are zero, and all others are negative. This corresponds to a T^2 torus.
- -3 to -6: Increasing numbers of zero Lyapunov-exponents, with all remaining exponents negative. These represent higher-dimensional invariant tori with quasi-periodic behavior.

As in most applications the dissipation has to be fairly small, we zoom in for $0 < b < 0.2$. We obtain the Lyapunov-exponents chart of fig. 25.

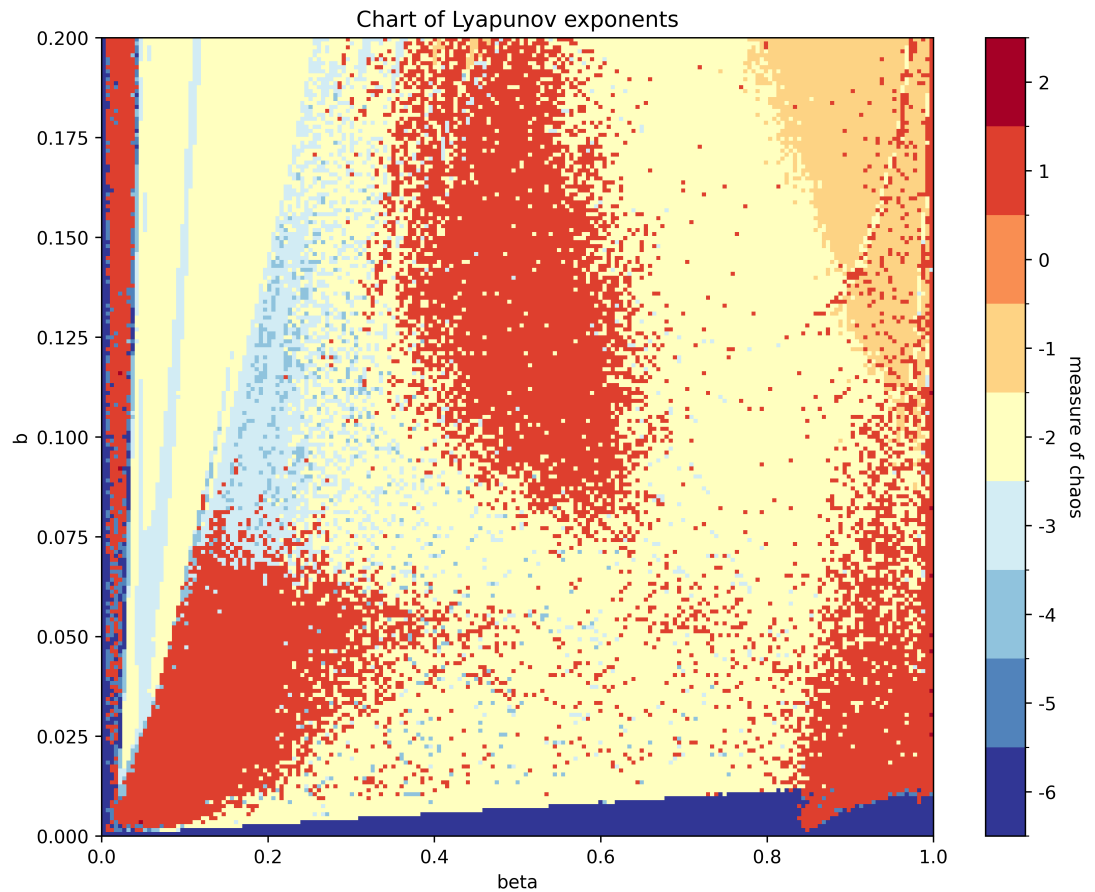


Figure 25. Parameter chart for $0 < b \leq 0.2$ and $0 < \beta \leq 1$, characterizing the interactions of two quasi-periodic oscillations based on Eq. (17), with fixed parameters $a_1 = 0.015$, $a_2 = 0.025$, and $c = 1$. The initial conditions are: $q_1 = 0$, $v_1 = 0.06955254625606$, $q_2 = 0.03492489869658$, $v_2 = -0.02743019598001$, $z_1 = 1.66213345371198$, and $z_2 = -0.03710401127306$. The coloring scheme used corresponds to a classification based on the number of zero Lyapunov exponents, with a threshold of 10^{-3} : any exponent with absolute value below this threshold is treated as zero. The values of the exponents, ranging from -6 to 2, are mapped to the *RdYlBu_r* colormap as follows: dark blue regions indicate the absence of clear dynamics, with all six Lyapunov exponents near zero (undecided behavior). Medium-dark blue corresponds to five exponents near zero, indicating a 5D torus, while medium blue (four near-zero exponents) corresponds to a 4D torus, and so on, with light blue corresponding to a 3D torus and yellow to a 2D torus, indicative of quasi-periodic behavior. Orange regions correspond to systems with one zero exponent, representing periodic orbits, while regions in red and dark red indicate chaotic or hyperchaotic dynamics, with one or two positive Lyapunov exponents. For the calculation of the Lyapunov coefficients, integration was performed from $t = 0$ to t_{\max} with a maximum time $t_{\max} = 1.5 \times 10^6$, and the expansion rates were calculated every 100 steps, resulting in 15,000 time steps used to compute the exponents.

4. Conclusions and Discussion

1. Our paper shows essentially an efficient hybrid approach. Analysis, in particular averaging-normalisation, and numerical bifurcation techniques go hand in hand. Fig. 15 is an example. The periodic solutions have been given by averaging and are indicated, the associated dynamics is added by numerics.
2. The use of nonlinear oscillators enables us to study isolated quasi-periodic interactions. For 2 components (section 3) the dynamics is essentially different from dissipative KAM theory.

381
382
383
384
385
386
387
388

3. Interaction of 2 components in the sense of section 3 is surprisingly rich producing periodic solutions, 2- and 3-tori, chaotic and hyper-chaotic behaviour.
4. Considering weak interactions and small oscillations one finds already this rich collection of bifurcations. The chart in Fig. 25 shows this for small b and β .
5. The thermostatic control used in the interacting systems originates from chemical physics. Applications of such a control to neural dynamics or economic models might be useful.
6. In the analysis of dynamics one can meet fractal manifolds that may show strange attraction. The use of Lyapunov-exponents for fractal manifolds presents basic problems; improvements in the use of these exponents to compute Kaplan-Yorke dimensions will be discussed in a forthcoming paper [5].

Author Contributions: Conceptualization, Validation, Writing – original draft, Taoufik Bakri and Ferdinand Verhulst.

Data Availability Statement: The data that support the findings of this study are available from the corresponding author upon reasonable request.

Acknowledgments: High precision numerics was obtained using MATCONT ode 78 under MATLAB.

Conflicts of Interest: The authors have no conflicts of interest.

Appendix A Periodic Chains of n Coupled Systems

One can extend system (17) to more than 2 coupled components but this poses a formidable problem. It is important to formulate in advance relevant questions for such complicated interacting chains especially the question if and how transmission of phenomena takes place in larger chains. This question has some relevance for neural dynamics. We restrict ourselves to some straightforward results. A few cases with $n = 4$ will be used for illustration.

Extending system (17) to n coupled systems and again simple direct coupling we have the periodic chain:

$$\begin{cases} \dot{q}_1 + bz_1\dot{q}_1 + q_1 &= -cq_1^3 + \beta q_n, \\ z_1 &= q_1^2 + \dot{q}_1^2 + \frac{c}{4}q_1^4 - a_1, \\ \dot{q}_2 + bz_2\dot{q}_2 + q_2 &= -cq_2^3 + \beta q_1, \\ z_2 &= q_2^2 + \dot{q}_2^2 + \frac{c}{4}q_2^4 - a_2, \\ \dots &\dots \\ \dot{q}_n + bz_n\dot{q}_n + q_n &= -cq_n^3 + \beta q_{n-1}, \\ z_n &= q_n^2 + \dot{q}_n^2 + \frac{c}{4}q_n^4 - a_n. \end{cases} \tag{A1}$$

The interaction constant $\beta > 0$ will determine the collective dynamics. In system (A1) the first component activates the second, the second one the third etc. The n^{th} component activates the first.

System (A1) can be written as a first order system $\dot{x} = F(x)$ in $3n$ -space with divergence:

$$Div F(x) = -b(z_1 + z_2 + \dots + z_n). \tag{A2}$$

As in section 3 the sign of the divergence will determine whether solutions will expand or contract locally.

Appendix A.1 Dynamics for Small Oscillations and Small Interactions

421

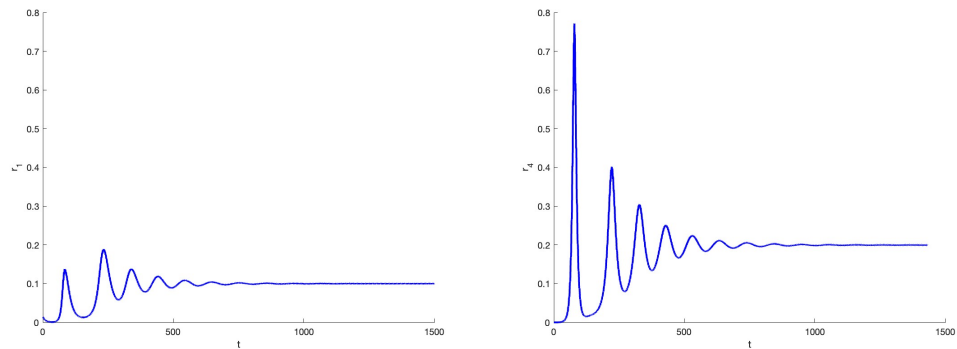


Figure A1. Dynamics of system (A1) for $n = 4$ and starting with small initial values. We have $a_1 = a_2 = 0.01, a_3 = a_4 = 0.04$. As predicted from the averaged equations (A3) $r_1(t), r_2(t)$ tend to the value 0.1, $r_3(t), r_4(t)$ tend to 0.2.

As in subsection 2.1 we scale $q_i = \sqrt{\varepsilon}x_i, \dot{q}_i = \sqrt{\varepsilon}\dot{x}_i, a_i \rightarrow \varepsilon a_i (i = 1, \dots, n), b = \varepsilon b_0$; consider small interactions by putting $\beta = \varepsilon \beta_0$. Introducing amplitude-phase coordinates $x_i = r_i(t) \cos(t + \phi_i(t)), \dot{x}_i = -r_i(t) \sin(t + \phi_i(t)), i = 1, \dots, n$ and averaging as in subsection 2.1 we find the $3n$ -dimensional system for $O(\varepsilon)$ approximations:

$$\begin{cases} \dot{r}_1 &= -\varepsilon(r_1 \frac{b_0}{2} z_1 + \frac{\beta_0}{2} r_n \sin(\phi_1 - \phi_n)), \dot{\phi}_1 = \varepsilon(\frac{3}{8} cr_1^2 - \frac{\beta_0 r_n}{2r_1} \cos(\phi_1 - \phi_n)), \\ \dot{z}_1 &= \varepsilon(r_1^2 - a_1), \\ \dot{r}_2 &= -\varepsilon(r_2 \frac{b_0}{2} z_2 + \frac{\beta_0}{2} r_1 \sin(\phi_2 - \phi_1)), \dot{\phi}_2 = \varepsilon(\frac{3}{8} cr_2^2 - \frac{\beta_0 r_1}{2r_2} \cos(\phi_2 - \phi_1)), \\ \dot{z}_2 &= \varepsilon(r_2^2 - a_2), \\ \dots &= \dots \\ \dot{r}_n &= -\varepsilon(r_n \frac{b_0}{2} z_n + \frac{\beta_0}{2} r_{n-1} \sin(\phi_n - \phi_{n-1})), \dot{\phi}_3 = \varepsilon(\frac{3}{8} cr_n^2 - \frac{\beta_0 r_{n-1}}{2r_n} \cos(\phi_n - \phi_{n-1})), \\ \dot{z}_n &= \varepsilon(r_n^2 - a_n). \end{cases}$$

For $n = 4$ a first illustration is presented in fig. A1 where we have small initial conditions and $a_1 = a_2 = 0.01, a_3 = a_4 = 0.04$.

Appendix A.2 Equal Combination Angles and Control Parameters a_i

A simple assumption is to choose in system (A3) the parameters $a_i, i = 1, \dots, n$ and the initial combination angles equal.

Critical values

For a critical point of system (A3) we require that $r_1 = \sqrt{a_1}, r_2 = \sqrt{a_2}, \dots, r_n = \sqrt{a_n}$. If initially $z_1 = z_2 = \dots = z_n = 0$ and $\phi_1 - \phi_n = 0, \pi; \phi_2 - \phi_1 = 0, \pi; \dots, \phi_n - \phi_{n-1} = 0, \pi$ the n amplitudes will be constant.

With these choices system (A3) will have a critical point (equilibrium) corresponding with a periodic solution of system (A1).

To illustrate this we choose $n = 4$, so $a_i = a, i = 1, \dots, 4$; the combination angles $\phi_1 - \phi_4 = \phi_2 - \phi_1 = \phi_3 - \phi_2 = \phi_4 - \phi_3$ and z_1, \dots, z_4 tend to the same values. We show that in this case we can extend the analysis to obtain critical points of the averaged system (A3) and so periodic solutions of system (A1).

Putting $z_n = 0, n = 1, \dots, 4$ for these critical point components we extend the symmetric solution discussed in subsection 2.1 to 4 components. Assuming constant amplitudes we need for the combination angles values $0, \pi$. Substitution of the amplitude and angle values

in the equations for the phases we find that the combination angles are constant. This leads to 2 critical points and so 2 periodic solutions. The eigenvalues of the first equilibrium (i.e. the one with combination angles equal to zero) are:

$$\begin{aligned} \lambda_{1...4} &= 0; \\ \lambda_{5,6} &= \pm i\sqrt{ab}; \\ \lambda_{7,8} &= \pm \frac{\sqrt{-a^8(4ab + 3a\beta + 4\beta^2)}}{2a^4}; \\ \lambda_{9,10} &= \pm \frac{\sqrt{-\frac{1}{2}a^9(8b + 3\beta) - \frac{1}{2}\sqrt{-a^{16}\beta^2(3a + 4\beta)^2}}}{2a^4}; \\ \lambda_{11,12} &= \pm \frac{\sqrt{\sqrt{-a^{16}\beta^2(3a + 4\beta)^2} - a^9(8b + 3\beta)}}{2\sqrt{2}a^4}. \end{aligned}$$

Using the parameters as in fig. A2 we find the first equilibrium is unstable.

$$\begin{aligned} \lambda_{1...4} &= 0; \\ \lambda_{5,6} &= \pm 0.316228i; \\ \lambda_{7,8} &= \pm 3.05369i; \\ \lambda_{9,10} &= \pm (-1.48406 + 1.55401i); \\ \lambda_{11,12} &= \pm (1.48406 - 1.55401i). \end{aligned}$$

In fig. A2 the instability of the first equilibrium (case 1) is shown; the solution starting near equilibrium 1 moves to equilibrium 2 (case 2) where the z-components tend to 1.

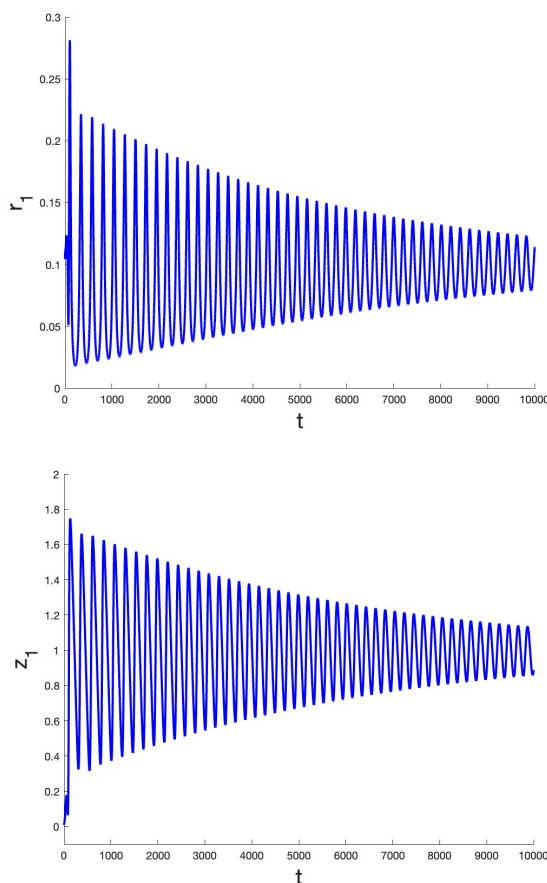


Figure A2. Dynamics based on system (A1) for $n = 4$ with projections $r_1(t)$ and $z_1(t)$ for 10 000 timesteps. The initial conditions are taken near the critical point of case 1: in vector form $q(0) = 0.11, 0.1, 0.11, 0.12; v(0) = 0, 0, 0, 0; z(0) = 0.01, 0, 0.01, -0.01$ with for the parameters $a = 0.01, b = 0.1, c = 1, \beta = 0.1$. The components $q(t), z(t)$ tend to the limiting values of case 2 (combination angles π).

Remark

A different type of solution with equal combination angles but the z -coordinates unequal zero is possible. The combination angles are constant if $\phi_1 - \phi_4 = \pi/2, 3\pi/2$. For r_1, \dots, r_4 to be constant we find

$$z_1 = z_2 = z_3 = z_4 = \pm \frac{\beta_0}{b_0}. \tag{A4}$$

This produces solutions with less symmetry. For the case $n = 4$ one can obtain explicit expressions with conditions for the parameters and for bifurcational behaviour.

References

1. Taoufik Bakri and Ferdinand Verhulst, *Bifurcations and quasi-periodic dynamics: torus breakdown*, Z. Angew. Math. Phys. 65, pp. 1053-1076 (2014).
2. T. Bakri, Y.A. Kuznetsov and F. Verhulst, *Torus bifurcations in a mechanical system*, J. Dyn. Diff. Equat. 27 pp. 371-403 (2015).
3. Taoufik Bakri and Ferdinand Verhulst, *Time-reversal, tori families and canards in the Sprott A and NE9 systems*, CHAOS doi: 10.1063/s.0097508 (August 2022).
4. Taoufik Bakri and Ferdinand Verhulst, *The dynamics of the Sprott B system*, CHAOS accepted for publ. (2024)
5. Taoufik Bakri and Ferdinand Verhulst, *A note on the Kaplan-Yorke dimension*, Int. J. Bif. Chaos (accepted for publ. 2025)
6. Stephen Boyd, *L-exponents*, in ChaosBook, Chaos: Classical and Quantum ch. 6 P. Cvitanović et al.(eds.) Chaosbook.org (2020)

7. H.W. Broer, G.B. Huitema, and M.B. Sevryuk, *em Quasi-periodic motions in families of dynamical systems*, Lecture Notes in Mathematics 1645, Springer (1996). 466
8. H.W. Broer, H. Hanssmann and F. Wagener, *Parametrised KAM theory, an overview*, preprint (2024). 467
9. M-C. Ciocci, A. Litvak-Hinenzon and H.W. Broer., *Survey on dissipative KAM theory including quasi-periodic bifurcation theory*, Geometric Mechanics and Symmetry: the Peyresq Lectures, 306, pp. 303-355 (2005). 468
10. E. Doedel, A.R. Champneys, T.F. Fairgrieve, Yu.A. Kuznetsov, B. Sandstede, and X.J. Wang, *AUTO97: Continuation and bifurcation software for ordinary differential equations* (with Hom-Cont), Concordia University, Montreal, Canada, silver edition, 1997. Download versions at GifHub and SourceForge. 469
11. M. Gräßer and T. Jäger, *Dimension of Attractors in Pinched Skew Products*, Commun. Math. Phys. 320, pp. 101-119 (2013). 470
12. P. Grassberger and I. Procaccia, *Measuring the strangeness of strange attractors*, Physica D, 9 pp. 189-208 (1983). 471
13. S. Jafari, J.C. Sprott and S. Golpayegani, *Elementary quadratic chaotic flows with no equilibria*, Physics Letters A 377, pp. 699-702 (2013). 472
14. A.P. Kuznetsov, S.P. Kuznetsov, N.A. Shchegoleva, N.V. Stankevich, *Dynamics of coupled generators of quasiperiodic oscillations: Different types of synchronization and other phenomena*, Physica D 398, pp. 1-12 (2019). 473
15. Yu.A. Kuznetsov, *Elements of Applied Bifurcation Theory*, 4th ed. Applied Math. Sciences 112, Springer (2023). 474
16. J.S.W. Lamb and J.A.G. Roberts, *Time-reversal symmetry in dynamical systems: A survey*, Physica D 112, pp. 61-39702 (1998). 475
17. J. Laskar. *Frequency analysis of a dynamical system*. Celestial Mechanics and Dynamical Astronomy 56, pp. 191–196, (1993). 476
18. MATCONT, Numerical continuation and bifurcation program, available at <http://www.matcont.ugent.be> 477
19. M. Messias and A.C. Reinol, *On the formation of hidden chaotic attractors and nested invariant tori in the Sprott A system*, Nonlinear Dyn. 88, pp.807-821 (2017). 478
20. M. Messias and A.C. Reinol, *On the existence of periodic orbits and KAM tori in the Sprott A system: a special case of the Nosé-Hoover oscillator*, Nonlinear Dyn. 92, pp. 1287-1297 (2018). 479
21. Henri Poincaré, *Les Méthodes Nouvelles de la Mécanique Céleste*, 3 vols. Gauthier-Villars, Paris, 1892, 1893, 1899. 480
22. J.A.G. Roberts and G.R.W. Quispel *Chaos and time-reversal symmetry. Order and chaos in reversible dynamical systems*, Physics Reports 216, pp. 63-177 (1992). 481
23. J.A. Sanders, F. Verhulst, F. and J. Murdock, *Averaging methods in nonlinear dynamical systems*, rev.ed. Springer-Verlag (2007). 482
24. C. Simo, *On the analytical and numerical approximation of invariant manifolds*, Modern Methods in Celestial Mechanics. Proceedings of 13th springschool on astrophysics (1989). 483
25. J.C. Sprott, *Technical Notes: Chaos in Time-Series Analysis*, online at: sprott.phys.wisc.edu, University of Wisconsin at Madison (2013). 484
26. J.C. Sprott, *Some simple chaotic flows*, Physical Review E 50, pp. R647-R650 (1994). 485
27. N.V. Stankevich, N.A. Shchegoleva, I.R. Sataev, A.P. Kuznetsov, *Three dimensional torus breakdown and chaos with two zero Lyapunov exponents in coupled radio-physical generators*, J. Comp. Nonl. Dynamics 15, issue 11, (nov. 2020), doi.org/10.1115/1.4048025 486
28. F. Takens, *Reconstruction Theory and Nonlinear Time Series Analysis*, Handbook of Dynamical Systems vol. 3 (H.W. Broer, B. Hasselblatt and F. Takens, eds.) pp. 345-377 (2010). 487
29. A.N. Tikhonov, *Systems of differential equations containing a small parameter multiplying the derivative* (in Russian), Math. Sb. 31 (73), 575-586 (1952). 488
30. A. Tondl, *On the interaction between self-excited and parametric vibrations*, National Research Institute for Machine Design, Běchovice, Monographs and Memoranda 25, Prague (1978). 489
31. M.E. Tuckerman, *Statistical Mechanics: theory and molecular simulation*, Oxford University Press (2010), (2nd ed. 2017). 490
32. Ferdinand Verhulst, *Nonlinear differential equations and dynamical systems* 2nd ed., Springer, New York etc., (2000). 491
33. Ferdinand Verhulst, *Methods and applications of singular perturbations*, Springer, New York etc., (2005). 492
34. Ferdinand Verhulst, *A Toolbox of Averaging Theorems, ordinary and partial differential equations*, Surveys and Tutorials in the Applied Mathematical Sciences, Springer (2023). 493

Disclaimer/Publisher's Note: The statements, opinions and data contained in all publications are solely those of the individual author(s) and contributor(s) and not of MDPI and/or the editor(s). MDPI and/or the editor(s) disclaim responsibility for any injury to people or property resulting from any ideas, methods, instructions or products referred to in the content. 510